Journal of Information Hiding and Multimedia Signal Processing ©2017 ISSN 2073-4212
Ubiquitous International Volume **8**, Number **4**, July **2017**

Multi-scale Application of Camera Calibration in Tourism Service Platforms

Xintao Ding[1,2,*], Yonglong Luo[2,*], Guorong Cai[3], and Xiaobo Zhang[4]

[1]School of Territorial Resources and Tourism
Anhui Normal University
No. 819 South Jiuhua Road, Wuhu, 241002, China
[2]School of Mathematics and Computer Science
Anhui Normal University
No. 819 South Jiuhua Road, Wuhu, 241002, China
[*]Corresponding Author
E-mail: xintaoding@163.com, ylluo@ustc.edu.cn
[3]Computer Engineering College
Jimei University
No. 183 Yinjiang Road, Xiamen, China
[4]Institute of Graphics and Image Processing
Xianyang Normal University
No. 43 Wenlin Road, Xianyang, China

Received February, 2016; revised January, 2017

Abstract. *Full view panoramas are able to simulate tele-presence or virtual reality experience, thus panoramic technology is an important implementation approach for the visual expression of tourism service platforms (TSP). On one hand, camera calibration, which is generally implemented under a certain resolution, may be a necessary preprocessing stage for panoramic technology. On the other hand, multi-scale applications are potentially involved in TSP for visualization expression. Therefore, calibration parameters resulting in one scale should be extended to multi-scale applications, but the extension research on this topic is insufficient. In this paper, the relations of intrinsic and distortion calibration parameters under different scales were both presented. Then, based on these two claims, a multi-scale correction algorithm is proposed. After demonstration experiments, with the help of the algorithm, different scale panoramas were employed for visualization expression in TSP. The multi-scale application of camera calibration in TSP is beneficial to bring intuition feelings to tourists.*
Keywords: Multi-scale technology, Camera calibration, Tourism service platforms

1. **Introduction.** Tourism service platforms (TSP), which emphasize visualization, have been involved in many tourism applications, such as web guides [1], mobile intelligent tour guides [2], and smart cities [3]. Full view panorama images can simulate tele-presence or a virtual reality experience, so it may bring immersion feelings to tourists. Panoramic technology is an important implementation approach for the visual expression of TSP [4, 5]. However, panoramic image application in tourism is still insufficient [4, 5]. Although a large amount of computer literature has been aimed at panoramic technology, stitching technology was the primary research topic [6-9].

For panoramic technology, camera calibration may be a necessary preprocessing stage. Panoramic imaging may be implemented in an easy way after the distortions of the stitching images are corrected using calibration parameters. Generally, images used for stitching should be geometrically corrected before application.

To meet the design requirement of TSP, geometrical distortions should be corrected under different resolutions; however, camera calibration is generally implemented under a certain resolution. Therefore, camera parameters resulting in one scale should be extended to multi-scale. Much calibration research focused on accuracy [10], efficiency [11] and automation [12], but little attention has been paid to multi-scale applications. The extension of calibration parameters resulting in one scale to another scale is important to TSP.

In this paper, a multi-scale correction method is proposed in Section 2. Then, bearing in mind the proposed algorithm in Section 2, experiments are carried out for a fundamental demonstration in Section 3. In Section 4, the multi-scale method is applied in the design of TSP, in which the closely shot images with a lower scale are corrected using a calibration result obtained from higher scale pattern images, and the full view panoramas with higher scale are corrected using the same calibration result in a similar way. Finnally, some discussion and conclusions follow in Section 5.

2. **The Proposed Method.** For the sake of convenience, we model the multi-scale topic within a pyramid framework. Let I_0 be an original image. $\{I_0, I_1, \cdots, I_L\}$ be a pyramid sequence constructed from I_0. I_{k+1}, which is an image at the $k+1^{th}$ level of the pyramid and is derived from I_k by reducing the resolution by one-half. It can be seen that the higher the level in the pyramid, the higher the scale and the lower the resolution.

The basic pinhole camera model (Figure 1a) is principally designed for charge-coupled device (CCD) sensors. Let (u, v) be the projected pixel coordinates in the image, (X, Y) be the corresponding physical coordinates after centralization (Figure 1b), the physical size of every pixel along the X-axis and the Y-axis be dX and dY, respectively. The transformation between the physical and pixel coordinates may be presented as

$$\begin{pmatrix} u \\ v \\ 1 \end{pmatrix} = \begin{pmatrix} \frac{1}{dX} & 0 & u_0 \\ 0 & \frac{1}{dY} & v_0 \\ 0 & 0 & 1 \end{pmatrix} \begin{pmatrix} X \\ Y \\ 1 \end{pmatrix}, \tag{1}$$

where $(u_0, v_0) = (M/2, N/2)$ is the center pixel in the image plane, as shown in Figure 1b, and M and N are the row and column numbers of the image, respectively. It can be deduced that

$$\begin{aligned} (u_{0_{k+1}}, v_{0_{k+1}})^T &= (M_{k+1}/2, N_{k+1}/2)^T \\ &= (M_k/2, N_k/2)^T/2 \\ &= (u_{0_k}, v_{0_k})^T/2, \end{aligned} \tag{2}$$

where $(u_{0_{k+1}}, v_{0_{k+1}})$ is the center pixel of I_{k+1}; M_{k+1} and N_{k+1} are the row and column numbers of I_{k+1}, respectively; (u_{0_k}, v_{0_k}), M_k, and N_k have the similar senses.

Let $P = (x, y, z)$ be a fixed space point (Figures 1a and 1c), then its projection point p on the image plane is $(X, Y) = (fx/z, fy/z)$ in physical units, as shown in Figure 1c, where f is the focal length in physical units. When the image is down sampled one time, the pixel length is doubled, and the pixels number reduced by one-half, i.e.,

$$\begin{cases} dX_k = dX_{k+1}/2 \\ dY_k = dY_{k+1}/2, \end{cases} \tag{3}$$

where dX_k and dY_k are the physical size of every pixel along the X-axis and Y-axis of I_k, respectively. Similarly, dX_{k+1} and dY_{k+1} exist.

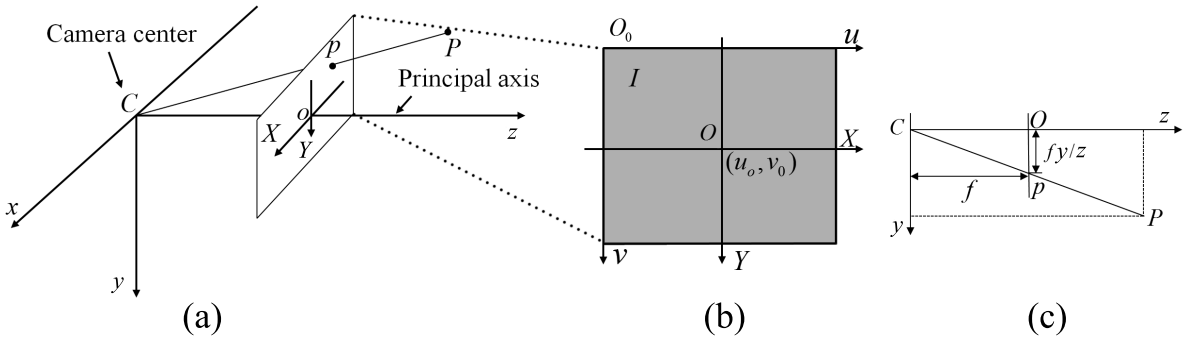

FIGURE 1. Camera system. (a) Pinhole camera model. C is the camera center and O is the principal point. XOY is the image plane. (b) Image and camera coordinate systems. (c) Pinhole projection imaging on the yCz plane.

From [13], the intrinsic parameters may be represented as

$$\begin{pmatrix} \alpha & \gamma & u_0 \\ 0 & \beta & v_0 \\ 0 & 0 & 1 \end{pmatrix} = \begin{pmatrix} 1/dX & s & u_0 \\ 0 & 1/dY & v_0 \\ 0 & 0 & 1 \end{pmatrix} \begin{pmatrix} f & 0 & 0 \\ 0 & f & 0 \\ 0 & 0 & 1 \end{pmatrix} \tag{4}$$

where α and β are scale factors of the horizontal and vertical axes in the image, respectively; $s = \arctan\theta/dX$ is the skew, and $|\pi/2 - \theta|$ is the angle between the horizontal and vertical axes of the image plane [14].

Let the resulting intrinsic parameters of I_k be $A_k = \begin{pmatrix} \alpha_k & \gamma_k & u_{0_k} \\ 0 & \beta_k & v_{0_k} \\ 0 & 0 & 1 \end{pmatrix}$, then for the intrinsic parameters A_{k+1} of I_{k+1}, combining equations (2)-(4), we have

$$\begin{aligned} A_{k+1} &= \begin{pmatrix} \alpha_{k+1} & \gamma_{k+1} & u_{0_{k+1}} \\ 0 & \beta_{k+1} & v_{0_{k+1}} \\ 0 & 0 & 1 \end{pmatrix} \\ &= \begin{pmatrix} 1/dX_{k+1} & s_{k+1} & M_{k+1}/2 \\ 0 & 1/dY_{k+1} & N_{k+1}/2 \\ 0 & 0 & 1 \end{pmatrix} \begin{pmatrix} f & 0 & 0 \\ 0 & f & 0 \\ 0 & 0 & 1 \end{pmatrix} \\ &= \begin{pmatrix} 1/(2dX_k) & \arctan\theta/(2dX_k) & M_k/4 \\ 0 & 1/(2dY_k) & N_k/4 \\ 0 & 0 & 1 \end{pmatrix} \begin{pmatrix} f & 0 & 0 \\ 0 & f & 0 \\ 0 & 0 & 1 \end{pmatrix} \\ &= \begin{pmatrix} \alpha_k/2 & \gamma_k/2 & u_{0_k}/2 \\ 0 & \beta_k/2 & v_{0_k}/2 \\ 0 & 0 & 1 \end{pmatrix} \end{aligned}$$

Therefore, the intrinsic parameters of $I_i (0 \le i \le L)$ may be obtained from

$$A_i = \begin{pmatrix} 2^{k-i}\alpha_k & 2^{k-i}\gamma_k & 2^{k-i}u_{0_k} \\ 0 & 2^{k-i}\beta_k & 2^{k-i}v_{0_k} \\ 0 & 0 & 1 \end{pmatrix}, \tag{5}$$

From [15], the radial distortion parameter $K = (K(1), K(2))^T$ satisfies $DK = d$, i.e.,

$$\begin{pmatrix} (u-u_0)r^2 & (u-u_0)r^4 \\ (v-v_0)r^2 & (v-v_0)r^4 \end{pmatrix} \begin{pmatrix} K(1) \\ K(2) \end{pmatrix} = \begin{pmatrix} du \\ dv \end{pmatrix} \tag{6}$$

where (u, v) is the ideal observed image coordinates; $r^2 = (x/z)^2 + (y/z)^2$, $P = (x, y, z)$ is a world space point; $du = u^* - u$, $dv = v^* - v$, (u^*, v^*) is the real observed image coordinates. For the radial distortion parameters, we have Theorem 2.1.

Theorem 2.1. *In the pyramid image, let the lens radial distortion parameter of I_{k+1} be $K_{k+1} = (K_{k+1}(1), K_{k+1}(2))^T$. Then, the lens distortion parameter of I_k satisfies $K_k = K_{k+1}$.*

Proof: From equations (1)-(2), we have

$$u_{k+1} - u_{0_{k+1}} = \frac{1}{2}(u_k - u_{0_k}), \tag{7}$$

Similarly,

$$v_{k+1} - v_{0_{k+1}} = \frac{1}{2}(v_k - v_{0_k}), \tag{8}$$

Combining equations (5)-(8), and because of $r_{k+1}^2 = (x/z)^2 + (y/z)^2 = r_k^2$, we have

$$\begin{aligned} D_{k+1} &= \begin{pmatrix} (u_{k+1} - u_{0_{k+1}})r_{k+1}^2 & (u_{k+1} - u_{0_{k+1}})r_{k+1}^4 \\ (v_{k+1} - v_{0_{k+1}})r_{k+1}^2 & (v_{k+1} - v_{0_{k+1}})r_{k+1}^4 \end{pmatrix} \\ &= \frac{1}{2}\begin{pmatrix} (u_k - u_{0_k})r_k^2 & (u_k - u_{0_k})r_k^4 \\ (v_k - v_{0_k})r_k^2 & (v_k - v_{0_k})r_k^4 \end{pmatrix} \\ &= \frac{1}{2}D_k \end{aligned} \tag{9}$$

Let $du_{k+1} = dx/dX_{k+1}$, where $dx = x^* - x$ is the physical error between the real and ideal normalized image coordinates. Then, we have

$$du_{k+1} = dx/dX_{k+1} = dx/(2dX_k) = du_k/2 \tag{10}$$

and

$$dv_{k+1} = dv_k/2. \tag{11}$$

Since $DK = d$, we have

$$K = (D^T D)^{-1} D^T d. \tag{12}$$

From equations (9)-(12), the radial distortion parameters of I_{k+1} should satisfy

$$\begin{aligned} K_{k+1} &= (D_{k+1}^T D_{k+1})^{-1} D_{k+1}^T d_{k+1} \\ &= (\frac{1}{4}D_k^T D_k)^{-1} \frac{D_k^T}{2} \frac{d_k}{2} \\ &= (D_k^T D_k)^{-1} D_k^T d_k \\ &= K_k. \end{aligned} \tag{13}$$

i.e.,

$$K_k = K_{k+1}.$$

With regard to the extrinsic parameters, they are determined by the relative orientation between camera and world coordinations. They are both in physical units and have nothing to do with the transformation between the pixel and physical units. Therefore, the extrinsic parameters remain the same regardless of image resolution.

Bearing in mind the calibration truths, image distortion correction under an arbitrary resolution may be implemented using Algorithm 1.

Algorithm 1 Image distortion correction under an arbitrary resolution.

Input:

An image I used for distortion correction with resolution $M_1 \times N_1$.

A group of calibration parameters obtained by the same camera under a resolution $M_2 \times N_2$, including intrinsic matrix A_k and distortion vector K_2.

Output:

A distortion corrected image of image I under resolution $M_1 \times N_1$.

1: Obtain an intrinsic parameter matrix A_l of image I using equation (5), where $2^{k-l} = M_1/M_2$; α_k, β_k, γ_k, u_{0_k}, and v_{0_k} in equation (5) are intrinsic parameters of input A_k.

2: Correct the pending image using A_l and K_2.

3. **Demonstration Results.** To evaluate the proposed results, a demonstration calibration experiment is conducted. Many camera calibration tools are available online, such as the OpenCV Calibration Tool [16], and the Camera Calibration Toolbox for MATLAB [17]. For convenience, the MATLAB Toolbox was used for calibration in this work. The employed model plane is a checkerboard pattern (Figure 2) containing $14 \times 10 = 140$ corner points (shown as the red points in Figure 2). Every checker is a square in size of $3cm \times 3cm$. The size of the pattern is $w \times h = 39cm \times 27cm$ (Figure 2). Ten pattern images with different poses were employed for calibration. The experimental camera was a Canon1100.

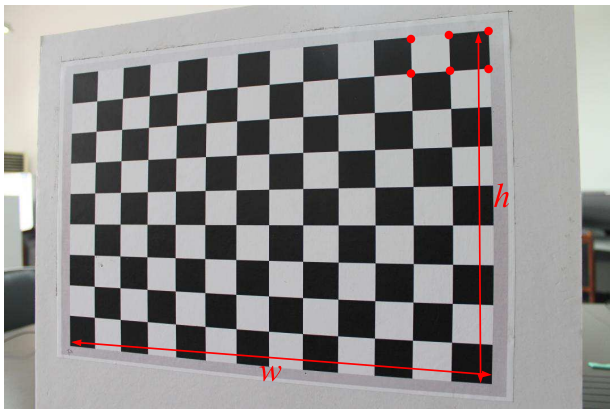

FIGURE 2. Calibration pattern. The red points show corner points; w and h are the width and height of the pattern, respectively.

In this section, two camera calibration experiments are implemented under two different resolutions to demonstrate whether the two calibration results stand by the two calibration truths presented in Section 2. Therefore, relative error is employed for evaluation. For intrinsic parameters, the parameters obtained from down sampled pattern images are zoomed at 2^{k-l} times so the comparison is implemented at a same scale, e.g., the relative error of focal length is defined as $e_f = (f_{I_l} - 2^{k-l} f_{I_k})/f_{I_l}$, where f_{I_l} and f_{I_k} are the focal lengths of the l-th level image I_l and k-th level image I_k in pyramid, respectively. Similarly, the relative error of the principal point is $e_p = (p_{I_l} - 2^{k-l} p_{I_k})/p_{I_l}$, where p_{I_l} and p_{I_k} are the coordinates of the principal points of the l-th level image I_l and k-th level image I_k in the pyramid, respectively. For the distortion parameters, the relative errors are defined the same as traditional relative errors, i.e., $e_d = (d_{I_l} - d_{I_k})/d_{I_l}$, where d_{I_l} and d_{I_k} are the distortion parameters of the l-th level image I_l and k-th level image I_k in the pyramid, respectively. The results of the two calibration experiments at resolutions 4272×2848 and 1068×712 are shown in Table 1. Because $2^{k-l} = 4272/1068 = 4$, the

aforementioned relative error may be obtained. The relative errors are listed in the fourth column in Table 1.

TABLE 1. Relative errors between the two calibration results under different resolutions.

Resolution	4272×2848	1068×712	Relative Error
Focal Length	(3554.55, 3554.79)	(891.071, 890.844)	(-0.0027, -0.0024)
Principal Point	(2161.5, 1432.37)	(539.418, 357.25)	(0.0018, -0.0024)
Distortion	(-0.155979, 0.147811)	(-0.157104, 0.149294)	(-0.0072, -0.0100)

From Table 1, the relative errors of the intrinsic parameters are no more than three thousandth. The approximate zero results demonstrated that the intrinsic parameters between original images at a 4272×2848 resolution and its down sampled images at a 1068×712 resolution have 4 times the differences. Moreover, the relative errors of the distortion parameters are also very small. All of the relative errors listed in Table 1 are small enough to support our aforementioned truths. In other words, when two calibration experiments are separately carried out, the resulting calibration parameters satisfy the two truths presented in Section 2.

4. **Application.** After demonstration experiments, we show a multi-scale application of camera calibration in TSP, in which panoramas are designed for landscape expression. Since the rotation of the camera is a translation of the cylinder, the panoramas in this paper are stitched on cylinder surfaces. Panoramic technology is a compound procedure, and the implementation scheme is not unique. Lowe formulated stitching as a multi-image matching problem [6] in which five modules, including feature matching, image matching, bundle adjustment, automatic panorama straightening, and gain compensation were involved. Szeliski warped images to a cylinder surface and then constructed the panoramic mosaics using translation [18]. Using these two methodologies, the stitch work implemented in this paper contains four procedures including geometrical correction, scale-invariant feature transform (SIFT) registration, random sample consensus (RANSAC) refining, and image stitching. Camera calibration was implemented as prepared work. Then, stitching images with different resolutions were geometrically corrected using the proposed Algorithm 1. After feature point extraction and SIFT and RANSAC refinement, stitching images were projected onto the cylinder surface with the radius equaling the focal length. Finally, images were stitched on the cylinder surface, and the output panoramas were unwrapped from the cylindrical surface to a plane. The parameters occurring in the SIFT and RANSAC modules were the default parameters of the SIFT demo program and the RANSAC toolbox for MATLAB as presented in [19] and [20], respectively.

Figure 3 shows the combinative implementation in TSP. The landscape of Figure 3 is Unity Pine of Mt. Huangshan, China. Figure 3a, which is the cylindrical panorama, delivers the surroundings of the Unity Pine. Figure 3b, which is the closely shot panoramic image, emphasizes the detail expression of the Unity Pine. To help tourists enhance intuition feelings, the close shot panorama in Figure 3b is designed to be a pop-up image as a click response of an interesting region (as shown the rectangle region in Figure 3a). The stitching image numbers of Figures 3a and 3b are 12 and 3, respectively, and they are all taken by the Canon 1100. The stitching images of Figure 3a are at a 534×356 resolution, while those in Figure 3b are at a 2136×1424 resolution. The scale of the closely shot panorama is lower than the full view photographs. Without the loss of generality, the calibration results of the Canon 1100 under a resolution of 1068×712 in Table 1

FIGURE 3. Visualization of the Unity Pine. (a) Full view panorama shows landscape context. (b) Closely shot panoramic image showing the Unity Pine in detail.

is taken for the reference parameters, which are adopted as the known parameters in Algorithm 1. Original stitching images of Figures 3a and 3b are geometrically corrected using Algorithm 1, where correction parameters are listed in Table 2. With the help of the other three modules, panoramas are produced as shown in Figures 3a and 3b.

TABLE 2. Correction parameters of the stitching images in Figures 3a and 3b.

Resolution	534×356	2136×1424
Focal Length	(445.536, 445.422)	(1782.142, 1781.688)
Principal Point	(269.7, 178.6)	(1078.9, 714.5)
Distortion	(-0.157104, 0.149294)	(-0.157104, 0.149294)

The TSP is a complex visualization system, and the multi-scale application of camera calibration favors the visualization expression for TSP. Compared with visualization expression in a single manner, Figure 3 expresses the landscape Unity Pine in a combinative visual manner. The TSP designed in this way brings more intuition feeling to tourists.

5. **Discussion and Conclusions.** Different from calibration literature aimed at accuracy, efficiency and automation, calibration parameters conversion formulas under different resolutions were proposed in this work. The topic of the multi-scale method is concerned with the application of panorama in TSP, and the application of the multi-scale method allows the number of camera calibration experiments to be reduced from repeatedly implementation under every different resolution to one implementation under a certain resolution. The reduction is beneficial to the multi-scale visualization of TSP.

The proposed method aimed to correct images after employing a single calibration experiment under a certain resolution rather than multiple calibration experiments under every resolution. The advantage of the proposed method is to simplify the implementation of panoramas with different scales.

In this paper, camera parameters resulting in one scale were extended to multi-scale. The associations of camera calibration results obtained under different resolutions were shown clearly. With the help of the extension, a distortion correction algorithm objecting

to arbitrary resolution was designed. With the help of the correction algorithm, different scale panoramas were employed for visualization expression in TSP. The multi-scale application of camera calibration in TSP is beneficial to bring intuition feelings to tourists.

Acknowledgments. This work is supported by the Doctoral Scientific Research Foundation of Anhui Normal University under Grant No. 2016XJJ118, the National Natural Science Foundation of China under Grant No. 61370050, 61672039, 61602009, 61401383.

REFERENCES

[1] E. Kupriyanova, P. Hutchings and E. Wong, A fully illustrated web-based guide to distinguish native and introduced polychaetes of Australia, *Management*, vol. 7, no. 3, pp. 305-312, 2016.

[2] A. Cacho, L. Mendes-Filho, D. Estaregue, B. Moura, N. Cacho, F. Lopes and C. Alves, Mobile tourist guide supporting a smart city initiative: a Brazilian case study. *International Journal of Tourism Cities*, vol. 2, no. 2, pp. 164-183, 2016.

[3] R. G. Hollands, Critical interventions into the corporate smart city. Cambridge Journal of Regions, *Economy and Society*, vol. 8, no. 1, pp. 61-77, 2015.

[4] N. Gonçalves, How panoramic photography changed multimedia presentations in tourism Human-Computer Interaction, *HCI Intelligent Multimodal Interaction Environments*, Beijing, China, pp. 862-871, 2007.

[5] L. Khirfan, Ornamented Facades and Panoramic Views: The Impact of Tourism Development on al-Salt's Historic Urban Landscape. *International Journal of Islamic Architecture*, vol. 2, no. 2, pp. 307-324, 2013.

[6] M. Brown and D. G. Lowe, Automatic panoramic image stitching using invariant features, *International journal of computer vision*, vol. 74, no. 1, pp.59-73, 2007.

[7] V. S. V. Devi, S. M. Prasad and H. G. Bhat, An efficient algorithm for image stitching based on scale-invariant feature transform, *International Journal of Engineering*, vol. 2, no. 2, pp. 2305-8269, 2013.

[8] S. Saeed, R. Hafiz, A. Rasul, M. M. Khan, Y. Cho, U. Park and J. Cha, A unified panoramic stitching and multi-projector rendering scheme for immersive panoramic displays. *Displays*, vol. 40, pp. 78-87, 2015.

[9] R. Y. Huang, L. R. Dung and T. S. Hong, A Two-Stage Algorithm of High Resolution Image Alignment for Mobile Applications. *Journal of Computer and Communications*, vol. 4,no. 4, pp. 36-51, 2016.

[10] J. Sun, X. Chen, Z. Gong, Z. Liu, and Y. Zhao, Accurate camera calibration with distortion models using sphere images. *Optics & Laser Technology*, vol. 65, pp. 83-87, 2015.

[11] X. L. Yang and S. P. Fang, Effect of field of view on the accuracy of camera calibration, *Optik - International Journal for Light and Electron Optics*, vol. 125, no. 2, pp. 844-849, 2014.

[12] Q. Sun and D. Xu, Self-calibration of multi-camera networks without feature correspondence between different cameras, *Optik - International Journal for Light and Electron Optics*, vol. 125, no. 13, pp. 3331-3336, 2014.

[13] R. Hartley and A. Zisserman (eds.),*Multiple view geometry in computer vision*, Cambridge university press, New York, 2003.

[14] W. Wang and H. Farid, Detecting re-projected video, *International Workshop on Information Hiding*, Santa Barbara, California, USA, pp. 72-86, 2008.

[15] Z. Y. Zhang, A flexible new technique for camera calibration, *Pattern Analysis and Machine Intelligence, IEEE Transactions on*, vol. 22, no. 11, pp. 1330-1334, 2000.

[16] OpenCV Calibration Tool, `http://docs.opencv.org/doc/tutorials/calib3d/camera_calibration/camera_calibration.html`.

[17] Camera Calibration Toolbox for Matlab, `http://www.vision.caltech.edu/bouguetj/calib_doc/download/index.html`.

[18] R. Szeliski and H. Y. Shum, Creating full view panoramic image mosaics and environment maps, *Proceedings of the 24th annual conference on Computer graphics and interactive techniques*, New York, USA, pp. 251-258, 1997.

[19] D. G. Lowe, Distinctive image features from scale-invariant keypoints, *International journal of computer vision*, Vol. 60, no. 2, pp. 91-110, 2004.

[20] M. Zuliani, *RANSAC for Dummies*, Vision Research Lab, University of California, Santa Barbara, 2009.